

hp-finite element method for simulating light scattering from complex 3D structures

Sven Burger,^{ab} Lin Zschiedrich,^a Jan Pomplun,^a Sven Herrmann,^b Frank Schmidt^{ab}

^a JCMwave GmbH, Bolivarallee 22, D-14050 Berlin, Germany

^b Zuse Institute Berlin (ZIB), Takustraße 7, D-14195 Berlin, Germany

This paper will be published in Proc. SPIE Vol. **9424** (2015) 94240Z, (*Metrology, Inspection, and Process Control for Microlithography XXIX*, DOI: 10.1117/12.2085795), and is made available as an electronic preprint with permission of SPIE. One print or electronic copy may be made for personal use only. Systematic or multiple reproduction, distribution to multiple locations via electronic or other means, duplication of any material in this paper for a fee or for commercial purposes, or modification of the content of the paper are prohibited. Please see original paper for images at higher resolution.

ABSTRACT

Methods for solving Maxwell's equations are integral part of optical metrology and computational lithography setups. Applications require accurate geometrical resolution, high numerical accuracy and/or low computation times. We present a finite-element based electromagnetic field solver relying on unstructured 3D meshes and adaptive hp-refinement. We apply the method for simulating light scattering off arrays of high aspect-ratio nano-posts and FinFETs.

Keywords: Scatterometry, optical metrology, computational metrology, computational lithography, 3D rigorous electromagnetic field simulations, finite-element methods, hp-FEM

1. INTRODUCTION

Optical metrology can be used to detect features sizes on a sub-nanometer level. In the semiconductor industry it is used in process control and in mask quality control for pushing performance of DUV and EUV lithography.¹ Numerical modelling is an important part of optical metrology setups in this field: measurement results are compared to simulation results of a parameterized model in order to quantitatively determine dimensions of the measured sample. With increasing complexity and decreasing feature sizes, the need for accurate optical

Corresponding author: S. Burger

URL: <http://www.jcmwave.com>

URL: <http://www.zib.de>

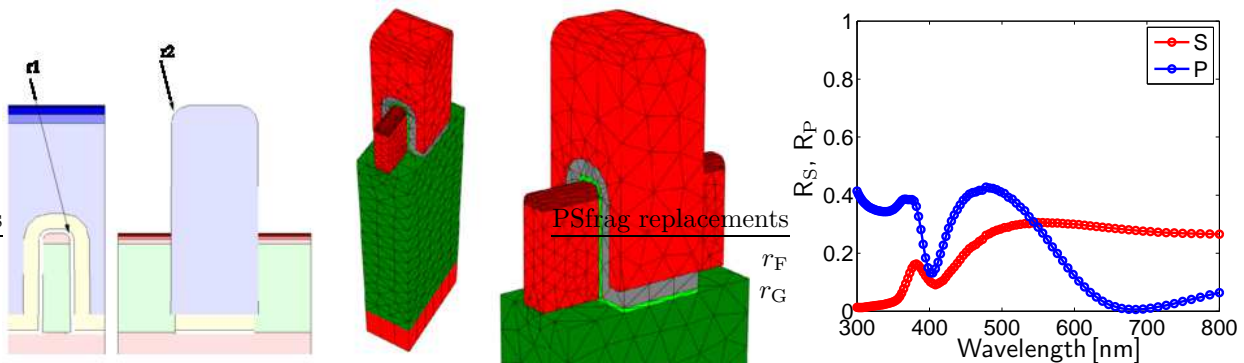


Figure 1. FinFET: *Left*: Images of the geometry layout in two cross-sections. *Center*: Images of parts of the tetrahedral mesh in different viewing directions. *Right*: Computed reflection spectra for S- and P-polarized light.

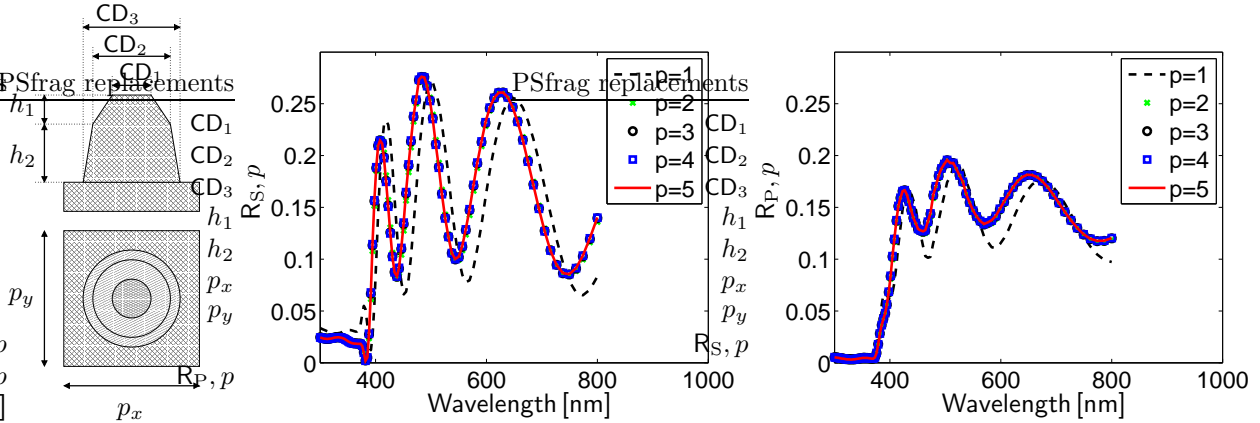


Figure 2. *Left*: Schematics of the geometry of the investigated scatterometric target (unit cell of a 2D-periodic grating of nano-posts with circular cross section, *not to scale*). Different parameters of the model are indicated (critical dimension, CD, at different heights, h_1 , h_2 , pitches p_x , p_y). *Center / right*: Reflection spectra of S/P-polarized light, $R_{S/P,p}$, for numerical discretization parameters $p = 1..5$.

metrology methods for complex 3D shapes is increasing.^{2,3} This triggers also a need for efficient numerical methods for computational metrology.

The challenge for electromagnetic field (EMF) solvers (Maxwell solvers) is typically efficiency (i.e., to achieve highly accurate results at low computation times). Finite-element methods (FEM) allow for high efficiency due to accurate geometrical modelling, adaptive meshing strategies, and higher-order convergence. In simulation tasks requiring high accuracy FEM can outperform other rigorous simulation methods.⁴⁻⁷

We develop and investigate finite-element methods for electromagnetic field simulations. In previous contributions these have been applied to various setups in optical metrology.⁸⁻¹⁵ In this context, also 3D structures have been investigated.¹⁶⁻¹⁹ Here we discuss methods for further performance improvements, especially for efficient simulation of 3D devices with complex geometries. This is reached by using hp-finite elements on unstructured, tetrahedral and prismatic meshes. Figure 1 shows the model, mesh, and simulation result of a typical investigated sample.

This paper is structured as follows: The background of the numerical method is presented in Section 2. The method is validated by presenting simulation results for two different examples related to current critical dimension (CD) metrology requirements.^{3,11} Section 3 presents simulations of nano-post arrays with high aspect-ratio. Section 4 presents simulations of arrays of fin field-effect transistors (FinFET).

2. HP FINITE ELEMENT METHOD

In the following the background of the finite element method is summarized.²⁰ Light scattering off nanoscopic structures on scatterometry samples is modeled by the linear Maxwell's equations in frequency domain.^{21,22} From these a single equation for the electric field \mathbf{E} can be derived:

$$\mathbf{curl} \mu^{-1} \mathbf{curl} \mathbf{E} - \omega^2 \epsilon \mathbf{E} = i\omega \mathbf{J}. \quad (1)$$

where ϵ and μ are the permittivity and permeability tensor, ω is the time-harmonic frequency of the electromagnetic field, and the electric current \mathbf{J} is source of an electromagnetic field. The domain of interest is separated into an infinite exterior Ω_{ext} which hosts the given incident field and the scattered field, and an interior Ω_{int} where the total field is computed. Electromagnetic waves incident from the exterior to the interior at the boundaries between both domains are added to the right hand side of Eq. (1). For numerical simulations the infinite exterior is treated using transparent boundary conditions (using the perfectly matched layer method, PML).

For a FEM discretization, Eq. (1) is first transformed into a weak formulation, i.e., it is tested with a vectorial function ϕ and integrated over \mathbb{R}^3 which yields:

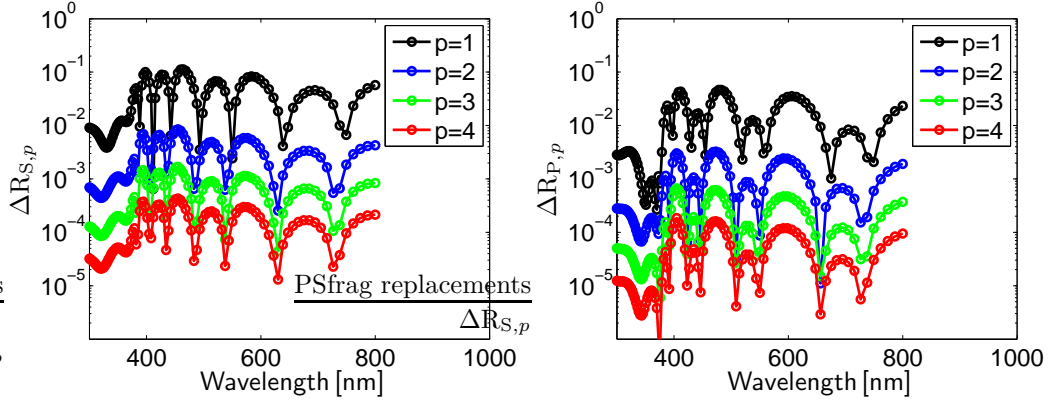


Figure 3. Spectral dependence of numerical discretization error $\Delta R_{S/P,p}$ for S/P polarization, obtained for various horizontal FEM degrees p , with fixed $p_z = 5$.

$$\int_{\mathbb{R}^3} \mathbf{curl} \phi \mu^{-1} \mathbf{curl} \mathbf{E} - \omega^2 \phi \varepsilon \mathbf{E} = i\omega \int_{\mathbb{R}^3} \phi \mathbf{J}. \quad (2)$$

For compact notation, the forms $a(\phi, \mathbf{E})$ and $f(\phi)$ are introduced, and the function space $H(\mathbf{curl})$ is defined.²⁰ The weak form of Maxwell's equations then reads:
Find $\mathbf{E} \in H(\mathbf{curl})$ such that:

$$a(\phi, \mathbf{E}) = f(\phi), \quad \forall \phi \in H(\mathbf{curl}). \quad (3)$$

A finite element discretization of Maxwell's equations restricts the formulation (3) to a finite-dimensional subspace V_h with $\dim V_h = N < \infty$:

Find $\mathbf{E}_h \in V_h$ such that:

$$a(\phi_h, \mathbf{E}_h) = f(\phi_h), \quad \forall \phi_h \in V_h. \quad (4)$$

Next, a basis $\{\varphi_1, \dots, \varphi_N\}$ of V_h is constructed, and the electric field is expanded using the basis elements: $\mathbf{E}_h = \sum_{i=1}^N e_i \varphi_i$. The variational problem (Eq. 4) is then tested with all elements of the basis which gives a linear system of equations:

$$\sum_{i=1}^N a(\varphi_j, \varphi_i) e_i = f(\varphi_j), \quad \forall j = 1, \dots, N. \quad (5)$$

The matrix $A_{ji} = a(\varphi_j, \varphi_i)$ is sparse and can be decomposed with efficient sparse LU solvers to obtain the unknown expansion coefficients e_i of the electric field.

The basis $\{\varphi_1, \dots, \varphi_N\}$ is constructed using elements φ_i (also called ansatz functions) which are polynomial functions of order p , and which are defined on a single patch of the spatial discretization of the geometry (mesh) only. For the results presented in this paper, we attribute elements of different polynomial order p to different patches of the mesh.²³ In regions where the mesh is very fine due to required geometry resolution (very thin layers or other fine details of the geometry) a lower polynomial order p can be chosen than in regions where the mesh is coarser. The method to distribute different orders p to the different patches relies on estimating errors on the different patches, making use of informations on geometry, meshing, material properties and source fields. This yields a basis $\{\varphi_1, \dots, \varphi_N\}$ which is well adapted to the problem and does not spend too much computational effort in regions where it is not required.

We demonstrate this so called *hp*-FEM method for two different applications: an array of very elongated posts and a transistor geometry with nanometer features (FinFET). For the array of nano-posts, due to the elongated geometry, best performance is reached when the mesh consists of elongated elements (in this case

prismatoidal elements) and when different polynomial degrees p are used in the dimension of elongation and in the orthogonal dimensions. For the transistor, an unstructured tetrahedral mesh discretizes the geometry, where the typical dimensions of the mesh elements, h , can vary over about two orders of magnitude. In this case different polynomial degrees p are used for different tetrahedral elements.

3. SIMULATION OF LIGHT SCATTERING OFF SILICON NANO-POSTS WITH HIGH ASPECT-RATIO

The model investigated in this section corresponds to a periodic array of Silicon nano-post on a silicon substrate. The geometrical setup is described schematically in Fig. 2 (left), and the parameter configuration for the simulations is defined in Table 1.

$p_x = p_y$	32 nm
$CD_1 / CD_2 / CD_3$	16 nm / 22 nm / 24 nm
h_1 / h_2	300 nm / 400 nm
θ / ϕ	30 deg / 0 deg

Table 1. Parameter settings for the Si nano-post array (compare Fig. 2).

In the model the structure is illuminated from above (superspace with refractive index $n = 1$) with S- and P-polarized plane waves, at an angle θ to the surface normal, and rotation angle ϕ . For simulating a wavelength spectrum, independent computations of the time-harmonic model for 100 wavelengths are performed. The optical material parameters of Silicon at each wavelength are obtained from tabulated data.²⁴ In our setup, up to 80 independent computations are processed in parallel on the computation threads of a standard workstation. Typical computation times for a single computation at low to medium accuracy levels range from below 1 sec to few seconds.

Fig. 2 (center, right) shows spectra of reflected S- and P-polarized light, R_S and R_P . The displayed spectra are obtained for the same physical setting, however, at different numerical resolutions p , i.e., $R_{S,p}$. In this case, we always use the same spatial mesh where the geometry is discretized using prismatoidal elements which are elongated in z -direction (surface normal). The numerical discretization parameter p here corresponds to the polynomial order of the finite-element ansatz functions φ_i (cf., Sec. 2) in the $x - y$ -plane. The polynomial order of the ansatz functions in z -direction in this case is chosen as $p_z = 5$. For the absolute values on a linear scale, as displayed in Fig. 2, differences in the computed spectra for $p > 2$ can hardly be detected. Therefore, in Figure 3 the differences of the computed spectra to the spectra computed at highest numerical resolution,

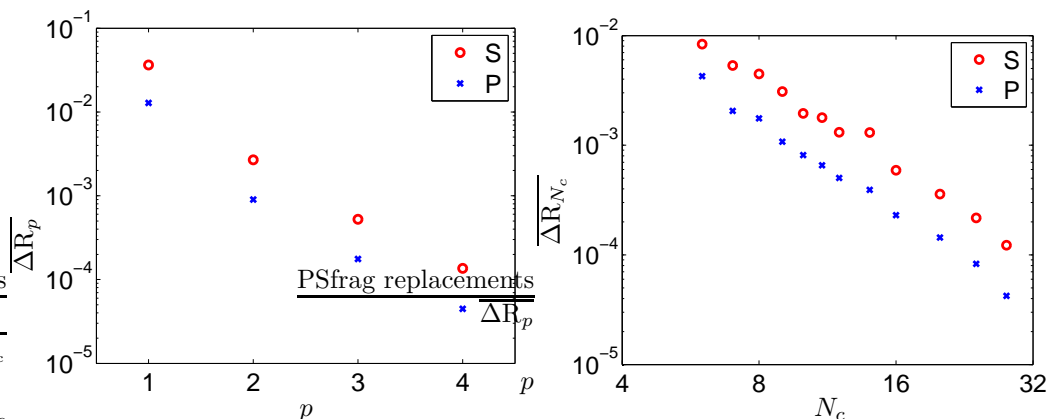


Figure 4. *Left:* Convergence of the average error $\overline{\Delta R_p}$ with horizontal finite element degree p , for S- and P-polarized incident light. *Right:* Convergence of the average error $\overline{\Delta R_p}$ with (geometrical) discretization parameter N_c (number of segments of the polygon defining the cross-section of the nano-post).

$\Delta R_{S,p} = |R_{S,p} - R_{S,p=5}|$, are displayed on a logarithmic scale. ΔR is also termed numerical discretization error. As can be expected the numerical discretization error decreases exponentially with p in the whole spectral range. We define the average discretization error as $\overline{\Delta R}_p = \sum_1^N \Delta R_p / N$, where the summation is performed over all N spectral points. Please note that several different conventions are used for defining numerical discretization errors in this context. The average error obtained from the data in Fig. 3 is displayed in Fig. 4 (left). In the investigated parameter regime, exponential convergence to very high accuracy levels is observed.

All results displayed in Figures 2 to 4 (left) are obtained on the same discretization of the geometry (essentially on the same prismatoidal mesh). In order to verify accuracy of the discrete geometry we have performed a convergence study for a meshing parameter: For meshing the nano-post geometry the mesh generator automatically discretizes the circular cross-section of the nano-post with a polygon, with a given number of segments, N_c . We have computed reflectivity spectra similar as in Fig. 2 for different segment numbers N_c . Here we have defined the average discretization error as $\overline{\Delta R}_{N_c} = \sum_1^N \Delta R_{N_c} / N$ with $\Delta R_{N_c} = |R_{N_c} - R_{N_c=36}|$. As can be seen from Fig. 4 (right) the results converge very well with geometry discretization parameter N_c . Results with an accuracy $\overline{\Delta R}_{N_c} < 0.2\%$ are obtained for $N_c \geq 10$.

4. SIMULATION OF LIGHT SCATTERING OFF FINFETS

The model investigated in this section corresponds to a periodic array of FinFET structures of the 22 nm (and smaller) technology nodes. Bunday *et al*³ point out that with the launch of such small structures on integrated circuits complex 3D architectures have become a crucial driver for down-scaling, and that this also implies additional needs for metrology.

The investigated geometrical setup is schematically shown in Fig. 1 (left). All dimensions of the device follow Fig. 15 and Table 10 of Bunday *et al*³ (22nm node: Fin pitch: 44 nm, Gate pitch: 88 nm, Fin width: 12.7 nm, Fin SWA: 89.5 deg, Fin height: 40 nm, Fin undercut: 2.1 nm, Gate width: 40 nm, Gate SWA: 89.8 deg, Gate height: 95 nm, Gate undercut: 2 nm, SiN thickness: 5 nm, High-k layer thickness: 2 nm, TiN thickness: 7 nm, BOX thickness: 200 nm). Additional parameters are roundings of the fin (r_F : 3 nm) and of the gate (r_G : 8 nm) top edges. The optical material parameters in the investigated spectral range are again obtained from tabulated data²⁴ (Si, SiN, SiO₂, TiN, TiO₂).

Fig. 1 (center) shows parts of tetrahedral meshes discretizing the FinFET geometry. Meshing is performed with an automatic mesh-generator,²⁵ which is a part of the finite-element package. The unstructured mesh allows to accurately resolve fine geometrical features like sub-nm undercuts, sidewall-angles and corner-roundings with only few additional mesh elements, facilitating accurate geometry modelling. When high refractive index contrasts between the different involved materials are present, such accurate geometry resolution is essential for

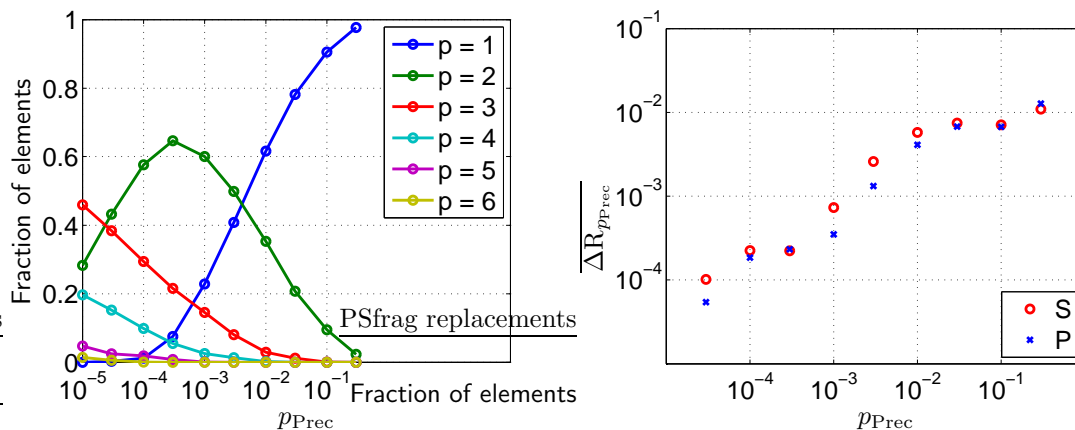


Figure 5. Hp-adaptive FinFET simulations: *Left*: Fraction of mesh elements on which ansatz functions φ_i with polynomial order p are used, as a function of the numerical accuracy parameter p_{Prec} . *Right*: Convergence of average numerical error $\overline{\Delta R}_{p_{Prec}}$ with accuracy parameter p_{Prec} .

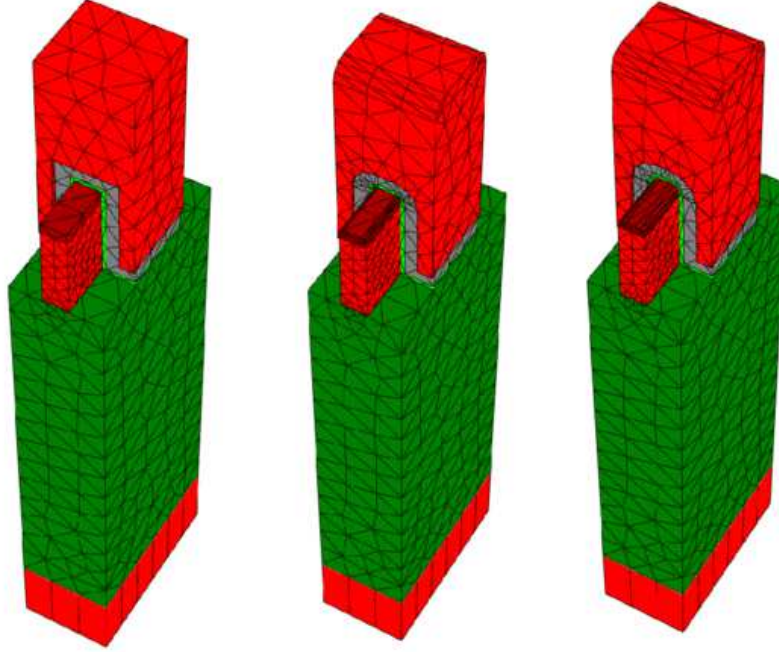


Figure 6. Tetrahedral meshes of the FinFET geometry with different settings of corner roundings: *Left*: No corner rounding, $r_F = 0$, $r_G = 0$. *Center*: $r_F = 1 \text{ nm}$, $r_G = 8 \text{ nm}$. *Right*: $r_F = 4 \text{ nm}$, $r_G = 8 \text{ nm}$.

precise approximation of the electro-magnetic field distributions. This enables accurate light scattering results in the far field, as inaccurate near-field resolution is generally not "smoothed out" in the far field. Computed reflection spectra for S- and P-polarized incident light at oblique angle of incidence are displayed in Fig. 1 (right).

The shortest dimensions of the edges of the tetrahedra in the meshes displayed in Fig. 1 (center) are comparable to the smallest geometrical features, i.e., typically smaller than 1 nm. However, for best performance, in regions of larger geometrical structures (e.g., in the gate, or in the buried oxide layer, etc.) mesh element dimensions are rather scaled with some fractions of the wavelength of light, i.e., several orders of magnitude larger than the dimensions of the smallest mesh elements.

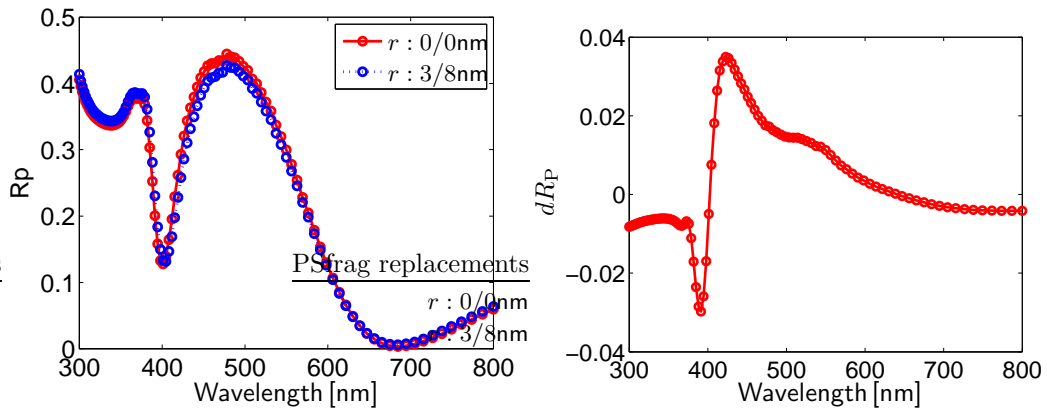


Figure 7. *Left*: Reflection spectra for P-polarized light, without corner rounding ($r_F = 0$, $r_G = 0$) and with corner rounding ($r_F = 3 \text{ nm}$, $r_G = 8 \text{ nm}$). *Right*: Difference between the two reflection spectra, $dR_P = R_P(r_F = 0, r_G = 0) - R_P(r_F = 3 \text{ nm}, r_G = 8 \text{ nm})$.

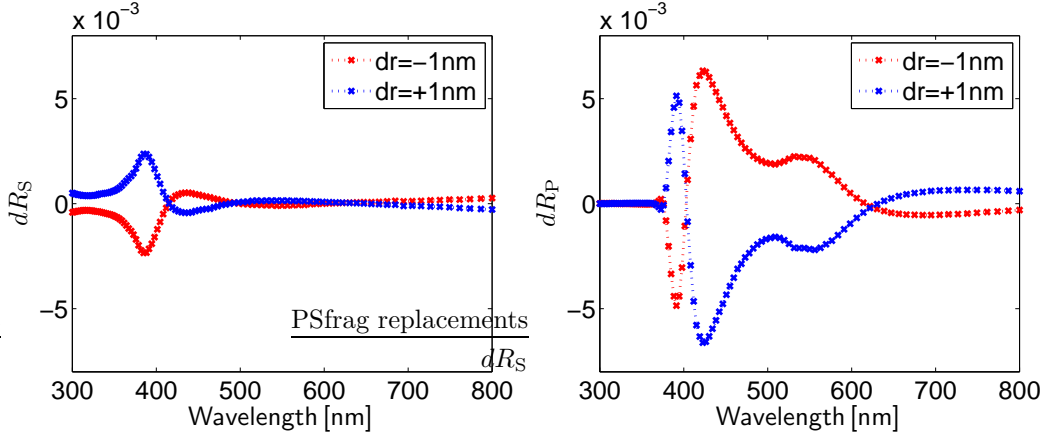


Figure 8. Spectral sensitivity of reflection of S (*left*) and P (*right*) polarized light for changes of fin corner rounding radius r_F around the value of $r_F = 3$ nm.

When assembling the finite-element matrix $A_{ji} = a(\varphi_j, \varphi_i)$ (cf. Eq. 5), a-priori error-estimation is used to choose the individual polynomial order p of the set of ansatz functions φ_i on each individual mesh element. A parameter p_{Prec} controls error-estimation. Figure 5 (left) shows how with different settings of p_{Prec} the fraction of mesh elements where different polynomial orders p are used is changing. E.g., for a setting of $p_{\text{Prec}} = 10^{-2}$ on about 60% of the mesh elements, ansatz functions φ_i with polynomial order $p = 1$ are used, on about 35% of the mesh elements, ansatz functions with $p = 2$ are used, and on the remaining elements, ansatz functions with $p \geq 3$ are used. With decreasing p_{Prec} these percentages shift towards higher p for the individual patches. Therefore, the dimension of A_{ji} increases with decreasing p_{Prec} , numerical discretization errors are expected to decrease with p_{Prec} , and computational costs increase with p_{Prec} , however, only moderately.²⁰ Figure 5 (right) shows convergence of the computed spectrum with p_{Prec} : very high accuracy levels are obtained.

Unstructured meshes and finite elements with adaptive (hp) choice of polynomial order p allows to obtain fast and accurate results. This allows to analyze and reconstruct fine geometry features for complex, multi-scale geometries. To demonstrate this we investigate the influence of corner rounding on scattering spectra. Bunday *et al*³ note fin corner rounding as a parameter which does influence FinFET performance. Figure 7 compares spectra for FinFET geometries with and without fin and gate corner roundings. Figure 8 shows the changes of S and P reflection spectra with fin corner rounding radius r_F . In these simulations, gate rounding was fixed to $r_G = 8$ nm, and fin rounding was varied by 1 nm around a rounding radius of $r_F = 3$ nm. The investigations can be used to design the scatterometric measurement setup for best sensitivity for specific parameters of interest.¹³ We note that sensitivities can also be computed directly at high accuracies.¹² Values of dR in Fig. 8 are of the order of up to few times 10^{-3} for changes of the rounding radius of 1 nm. This suggests that comparable or higher numerical accuracy ranges should be used in reconstructions of such parameters.

5. CONCLUSION

A finite-element method using hp-adaptivity on 3D prismatic and tetrahedral meshes has been demonstrated. Convergence to highly accurate results over a wide spectral range has been observed for examples related to CD metrology challenges. The method allows to efficiently compute scatterometric signals and sensitivities.

Acknowledgments

The presented work is part of the EMRP Joint Research Project IND 17 SCATTEROMETRY. The EMRP is jointly funded by the EMRP participating countries within EURAMET and the European Union. We thank Bernd Bodermann for discussions. We acknowledge the support of BMBF through project 13N13164 and of the Einstein Foundation through project ECMath OT5.

REFERENCES

- [1] Pang, L., Peng, D., Hu, P., Chen, D., He, L., Li, Y., Satake, M., and Tolani, V., “Computational metrology and inspection (CMI) in mask inspection, metrology, review, and repair,” *Adv. Opt. Techn.* **1**, 299 (2012).
- [2] Topol, A. W., La Tulipe, D.C., Shi, L., Frank, D., Bernstein, K., Steen, S., Kumar, A., Singco, G., Young, A., Guarini, K., and Ieong, M., “Three-dimensional integrated circuits,” *IBM J. Res. & Dev.* **50**, 491–506 (2006).
- [3] Bunday, B., Germer, T. A., Vartanian, V., Cordes, A., Cepler, A., and Settens, C., “Gaps analysis for CD metrology beyond the 22nm node,” *Proc. SPIE* **8681**, 86813B (2013).
- [4] Burger, S., Köhler, R., Zschiedrich, L., Gao, W., Schmidt, F., März, R., and Nölscher, C., “Benchmark of FEM, waveguide and FDTD algorithms for rigorous mask simulation,” *Proc. SPIE* **5992**, 599216 (2005).
- [5] Burger, S., Zschiedrich, L., Schmidt, F., Evanschitzky, P., and Erdmann, A., “Benchmark of rigorous methods for electromagnetic field simulation,” *Proc. SPIE* **7122**, 71221S (2008).
- [6] Hoffmann, J., Hafner, C., Leidenberger, P., Hesselbarth, J., and Burger, S., “Comparison of electromagnetic field solvers for the 3D analysis of plasmonic nano antennas,” *Proc. SPIE* **7390**, 73900J (2009).
- [7] Maes, B., Petráček, J., Burger, S., Kwicien, P., Luksch, J., and Richter, I., “Simulations of high-Q optical nanocavities with a gradual 1D bandgap,” *Opt. Express* **21**, 6794 (2013).
- [8] Scholze, F., Laubis, C., Dersch, U., Pomplun, J., Burger, S., and Schmidt, F., “The influence of line edge roughness and CD uniformity on EUV scatterometry for CD characterization of EUV masks,” *Proc. SPIE* **6617**, 66171A (2007).
- [9] Quintanilha, R., Sohn, Y., Barnes, B., Howard, L., and Silver, R., “Critical dimension measurements using a 193 nm scatterfield microscope,” *Proc. SPIE* **7390**, 73900S (2009).
- [10] Zang, L., Euser, T., Kang, M., Scharrer, M., and Russell, P. S. J., “Structural analysis of photonic crystal fibers by side scattering of laser light,” *Optics Letters* **36**(9), 1668 (2011).
- [11] Bodermann, B., Hansen, P.-E., Burger, S., Henn, M.-A., Gross, H. A., Bär, M., Scholze, F., Endres, J., and Wurm, M., “First steps towards a scatterometry reference standard,” *Proc. SPIE* **8466**, 84660E (2012).
- [12] Burger, S., Zschiedrich, L., Pomplun, J., Schmidt, F., and Bodermann, B., “Fast simulation method for parameter reconstruction in optical metrology,” *Proc. SPIE* **8681**, 868119 (2013).
- [13] Soltwisch, V., Burger, S., and Scholze, F., “Scatterometry sensitivity analysis for conical diffraction versus in-plane diffraction geometry with respect to the side wall angle,” *Proc. SPIE* **8789**, 878905 (2013).
- [14] Soltwisch, V., Wernecke, J., Haase, A., Probst, J., Schoengen, M., Krumrey, M., Scholze, F., Pomplun, J., and Burger, S., “Determination of line profiles on nano-structured surfaces using EUV and x-ray scattering,” *Proc. SPIE* **9235**, 92351D (2014).
- [15] Petrik, P., Kumar, N., Fried, M., Fodor, B., Juhasz, G., Pereira, S., Burger, S., and Urbach, H. P., “Fourier ellipsometry, an ellipsometric approach to fourier scatterometry,” *J. Europ. Opt. Soc. - Rap.* **10**, 15002 (2015).
- [16] Burger, S., Zschiedrich, L., Pomplun, J., and Schmidt, F., “Rigorous simulations of 3D patterns on extreme ultraviolet lithography masks,” *Proc. SPIE* **8083**, 80831B (2011).
- [17] Burger, S., Zschiedrich, L., Pomplun, J., Schmidt, F., Kato, A., Laubis, C., and Scholze, F., “Investigation of 3D patterns on EUV masks by means of scatterometry and comparison to numerical simulations,” *Proc. SPIE* **8166**, 81661Q (2011).
- [18] Kleemann, B. H., Kurz, J., Hetzler, J., Pomplun, J., Burger, S., Zschiedrich, L., and Schmidt, F., “Fast online inverse scattering with Reduced Basis Method (RBM) for a 3D phase grating with specific line roughness,” *Proc. SPIE* **8083**, 808309 (2011).
- [19] Kato, A., Burger, S., and Scholze, F., “Analytical modeling and 3D finite element simulation of line edge roughness in scatterometry,” *Appl. Optics* **51**, 6457 (2012).
- [20] Monk, P., [*Finite Element Methods for Maxwell’s Equations*], Oxford University Press (2003).
- [21] Pomplun, J., Burger, S., Zschiedrich, L., and Schmidt, F., “Adaptive finite element method for simulation of optical nano structures,” *phys. stat. sol. (b)* **244**, 3419 (2007).
- [22] Burger, S., Pomplun, J., and Schmidt, F., “Finite element methods for computational nano-optics,” in [*Encyclopedia of Nanotechnology*], Bhushan, B., ed., 837–843, Springer Netherlands (2012).

- [23] Babuška, I. and Dorr, M. R., “Error estimates for the combined h and p versions of the finite element method,” *Numer. Math.* **37**(2), 257–277 (1981).
- [24] Palik, E. D., [*Handbook of optical constants of solids*], Academic press (1985).
- [25] Blome, M., McPeak, K., Burger, S., Schmidt, F., and Norris, D. J., “Back-reflector design in thin-film silicon solar cells by rigorous 3D light propagation modeling,” *COMPEL: Int. J. Comput. Mathem. Electr. Electron. Eng.* **33**(4), 1282 – 1295 (2014).